Gas phase conformational basicity of carvedilol Fragment B, 2(S)-1-(ethylamonium)propane-2-ol: An ab initio study on a protonophoretic of oxidative phosphorylation uncoupling

ARTICLE *in* JOURNAL OF MOLECULAR STRUCTURE THEOCHEM · AUGUST 2003

Impact Factor: 1.37 · DOI: 10.1016/S0166-1280(03)00258-6

ELSEVIER

Journal of Molecular Structure (Theochem) 631 (2003) 251–270

THEO CHEM

www.elsevier.com/locate/theochem

Gas phase conformational basicity of carvedilol Fragment B, 2(*S*)-1-(ethylamonium)propane-2-ol: An ab initio study on a protonophoretic of oxidative phosphorylation uncoupling

David R.P. Almeida[a,*], Donna M. Gasparro[a], Luca F. Pisterzi[a], Ladislaus L. Torday[b], Andras Varro[b], Julius Gy. Papp[b,c], Botond Penke[d,e]

[a]*Department of Chemistry, Lash Miller Laboratories, University of Toronto, 80 St. George Street, Toronto, Ont., Canada M5S 3H6*
[b]*Department of Pharmacology and Pharmacotherapy, Szeged University, Dom ter 12, Szeged 6701, Hungary*
[c]*Division of Cardiovascular Pharmacology, Hungarian Academy of Sciences and Szeged University, zDom ter 12, Szeged 6701, Hungary*
[d]*Institute of Medical Chemistry, Szeged University, Dom ter 8, Szeged 6720, Hungary*
[e]*Hungarian Academy of Sciences, Protein Chemistry Research Group, University of Szeged, Dom ter 8, Szeged 6720, Hungary*

Received 13 January 2003; accepted 31 March 2003

Abstract

Carvedilol is cardiovascular drug of proven efficacy. It is believed that carvedilol exerts cardio-protective effects by acting as a mild uncoupler of mitochondrial oxidative phosphorylation, thereby protecting mitochondria from oxidative stress and preserving proper bioenergetics and cardiac function. This uncoupling occurs via a proton-shuttling mechanism involving the amino group of carvedilol's side-chain. However, the molecular details of carvedilol's proton affinity have not yet been completely worked out, especially with regards to the attributes of molecular conformation. In the present study, the full conformational basicity of a fragment of carvedilol, 2(*S*)-1-(ethylamonium)propane-2-ol (Fragment B), is presented to illustrate the protonophoretic character of carvedilol. Full gas phase geometry optimizations were performed at the ab initio, RHF/3-21G, level of theory for the entire potential energy hypersurface (PEHS) of Fragment B. Subsequently, since deprotonation can occur via two different protons, a two-prong methodology was applied to calculate vertical and adiabatic energies of deprotonation. A total of 18 out of a possible 81 minima converged and the dominant characteristic in all protonated and deprotonated conformers was a *gauche* plus effect in the rotation about the C–OH bond at the Fragment B stereocentre. Optimized energies of deprotonation ranged from 245 to 262 kcal mol^{-1} while protons involved in internal hydrogen bonding required an extra 6–8 kcal mol^{-1} for deprotonation compared to protons that were oriented away from the backbone structure. The overall trend indicates that conformers devoid of significant stabilization interactions possessed lower energies of deprotonation; in other words, as the relative conformer energy increased, vertical and adiabatic energies of deprotonation tended to decrease. Thus, extrapolating to carvedilol and the proton transfer mechanism involved in oxidative phosphorylation uncoupling, events of deprotonation will favour molecular conformations with minimal intramolecular stabilization and with higher relative energies.

* Corresponding author.
E-mail addresses: dalmeida@medscape.com (D.R.P. Almeida), dgasparro@medscape.com (D.M. Gasparro), lpisterzi@medscape.com (L.F. Pisterzi), pyro@phcol.szote.u-szeged.hu (L.L. Torday), varro@phcol.szote.u-szeged.hu (A. Varro), papp@phcol.szote.u-szeged.hu (J.G. Papp).

0166-1280/03/$ - see front matter © 2003 Elsevier B.V. All rights reserved.
doi:10.1016/S0166-1280(03)00258-6

Keywords: Carvedilol; 2(*S*)-1-(ethylamonium)propane-2-ol; Basicity; Proton affinity; Ab initio

1. Introduction

1.1. Medical Background

The cardiovascular drug carvedilol, 1-(9H-Carbazol-4-yloxy)-3-[2-(2-methoxy-phenoxy)ethylamino]-2-propanol ($C_{24}H_{26}N_2O_4$), is used in the treatment of mild to moderate congestive heart failure (CHF), essential hypertension, angina, and in improvement of left ventricular function [1]. Indicative of carvedilol's efficacy is the fact that the US Data and Safety Monitoring Board stopped, for ethical reasons, the clinical trials of carvedilol before its completion due to greatly lowered morbidity and mortality rates [2,3].

Carvedilol is a lipophilic autonomic nervous system agent that acts as a multiple-action neurohormonal antagonist by producing nonselective beta-blockage (β_1 and β_2), selective alpha-blockage (α_1), while also possessing myocardial-protective antioxidant properties [1,4]. By blocking the activity of cardiac β-adrenergic receptors (β_1 and β_2) to noradrenaline, carvedilol reduces cardiac output and oxygen consumption, and therefore, total cardiac work-load of the heart [5,6]. Carvedilol also provides positive effects by vasodilation (α_1-adrenergic blockage) at peripheral resistance vessels, which decreases preload and after-load, thereby reducing cardiac work and wall tensions [7].

As an antioxidant, the carbazole ring gives carvedilol and its metabolites a powerful tendency to donate electrons to 'scavenge' the activities of reactive oxygen species (ROS) such as: oxygen superoxide (O_2^-), hydrogen peroxide (H_2O_2), hydroxyl radical (·OH), and peroxynitrite ($ONOO^-$), and therefore, helps to protect the living body from the deleterious effects of free radical damage [8]. The free radical scavenging ability of carbazole, such as that seen against lipid peroxidation, is enhanced by its high lipid solubility [9].

Carvedilol has been shown to act as a novel anti-fibrillar agent and may have uses in the prevention of Alzheimer's; a disease characterized by neuronal cell loss associated with fibril formation [10]. Fibril formation leading to neuritic plaques occurs due to the aggregation of β-amyloid peptide (Aβ, 39–43 residue peptide) and it is generally accepted that preventing the conversion of Aβ peptides into biologically active fibrils may provide a method for slowing Alzheimer's neurotoxicity and pathology. The effectiveness of carvedilol's inhibition of Aβ fibril formation is due to three factors: (1) one central basic amino pharmacophore, (2) two cyclic hydrophobic ring centroids, and (3) the molecular flexibility to adopt a specific three-dimensional pharmacophore conformation [10]. However, it is currently not known if fibril inhibition occurs via carvedilol binding directly to Aβ monomers or to small oligomers [10].

1.2. Biological background

One of the cardio-protective effects of carvedilol resides in its ability to protect mitochondria from oxidative stress. This occurs by mild uncoupling of oxidative phosphorylation via the protonable amino group of carvedilol's side-chain [11]. Mitochondrial bioenergetics are involved in both physiological and pathological conditions since cardiac function is closely related to mitochondrial output. Due to the high demand of ATP from working cardiac muscles, a constant mitochondrial input is required. A compromise of mitochondrial bioenergetics leads to adverse consequences such as a failure to maintain calcium homeostasis which triggers apoptotic and necrotic pathways of cell death and suppresses delivery of ATP to heart muscles [12]. Uncouplers of oxidative phosphorylation are defined as chemical agents that selectively prevent the utilization of chemical energy derived from respiratory electron transport for the net phosphorylation of ATP from ADP [13]. These agents decrease the moles of inorganic phosphate (P_i) used (into organically bound form) per atom of oxygen consumed, and therefore, decrease the P/O ratio to zero in the presence of substrate. However, respiration in the mitochondria continues, i.e. respiration-dependent ATP synthesis is eliminated but respiration itself is not inhibited [13].

Characteristics of uncouplers in isolated mitochondria include increased respiration, inhibition of mitochondria-catalyzed exchange reactions, greatly increased apparent ATPase activity, and osmotic swelling [13].

It has been proposed that carvedilol's amino group ($pK_a = 7.9$) decreases the mitochondrial electric potential via a weak protonophoretic mechanism and uncouples oxidative phosphorylation by picking up a proton in the low pH cytosolic leaflet of the inner mitochondrial membrane (mitochondrial intermembrane space) and then crosses the membrane in the positively-charged protonated form into the relatively higher pH mitochondrial matrix [11]. It is postulated that carvedilol is able to cross the membrane as a positively charged species because of its high lipid solubility and driven by the electric potential which is negative in the matrix with regards to the intermembrane space [11]. Carvedilol then releases the proton in the matrix and returns to the cytosolic leaflet in the deprotonated neutral from [11]. The antioxidant activity of carvedilol in mitochondria may be due in part to this phenomenon known as 'mild uncoupling' in which a small decrease in mitochondrial electric potential induces a reduction in the ROS produced by the mitochondrial respiratory chain [11,14,15].

Thus, as described above, a proton-transfer process is ultimately responsible for the uncoupling in mitochondria by carvedilol. As such, it is necessary to explicitly define the molecular details of carvedilol's protonophoretic character. In this work, the intrinsic conformational basicity of 2(*S*)-1-(ethylamonium)propane-2-ol (Fragment B) will be analyzed because the function of proton affinity (basicity) and the willingness to give up a proton will correlate with the uncoupling effect on mitochondrial oxidative phosphorylation. Using a smaller model, possessing the same amino group in carvedilol's side-chain, the current investigators will illustrate the influence that carvedilol's molecular conformation exerts on its protonophoretics. An analysis of the entire conformational surface of Fragment B will be carried out because the diversity of effects in uncoupling found between carvedilol and its metabolite 3-hydroxyl carvedilol have been attributed to differences in molecular conformation [11], and therefore, it is essential to survey the entire conformational space.

1.3. Chemical background

Carvedilol contains one strereocentre and is commercially available as a racemic mixture of both its enantiomers (R[+] and S[−]) (c.f. Fig. 1). However, the enantiomers of carvedilol show marked stereoselective properties; both enantiomers have equal α_1 blocking activity and antioxidant activity but only the S[−] enantiomer contains the nonselective β-adrenergic blocking activity [16,17]. As such, neither enantiomer alone has the same pharmacologic profile as the racemic mixture of carvedilol used clinically. Moreover, carvedilol's metabolites (1-hydroxyl, 3-hydroxyl, and 8-hydroxyl carvedilol; c.f. Fig. 1) are potent antioxidants since a hydroxyl group substitution in a heterocyclic ring (such as carbazole) increases the molecular antioxidant action of a given compound [3,16,18,19]. Metabolites 1-hydroxyl and 3-hydroxyl carvedilol (c.f. Fig. 1) are also able to act as novel anti-fibrillar agents because they retain the needed pharmacophores and conformational flexibility [10]. This implicates that the conformational profile and intrinsic characteristics of carvedilol can be extrapolated to the structurally-analogous metabolites of carvedilol.

Carvedilol possesses three distinct pharmacophores, and therefore, was deconstructed into three structural fragments: *R*- and *S*-4-(2-hydroxypropoxy)carbazol (Fragment A) is responsible for the carbazole-related antioxidant effects of carvedilol, 2(*R* and *S*)-1-(ethylamonium)propane-2-ol (Fragment B) contains the protonophoretic amino group which connects the two oxygen-containing fragments of carvedilol, and aminoethoxy-2-methoxy-benzene (Fragment C) is responsible for the α-blocker action of carvedilol (c.f. Fig. 1). Beta-blockage is exerted by the composite of both Fragment A and B. While *R*- and *S*-4-(2-hydroxypropoxy)carbazol (Fragment A) has been studied [20], the current objective is the investigation of Fragment B.

2. Computational method

Fragment B was constructed with four torsional angles and the conformers of its potential energy hypersurface (PEHS) can be described according to Eq. (1) (c.f. Fig. 2). Newman projections display possible conformations of H12 (χ_{10} torsional angle) at

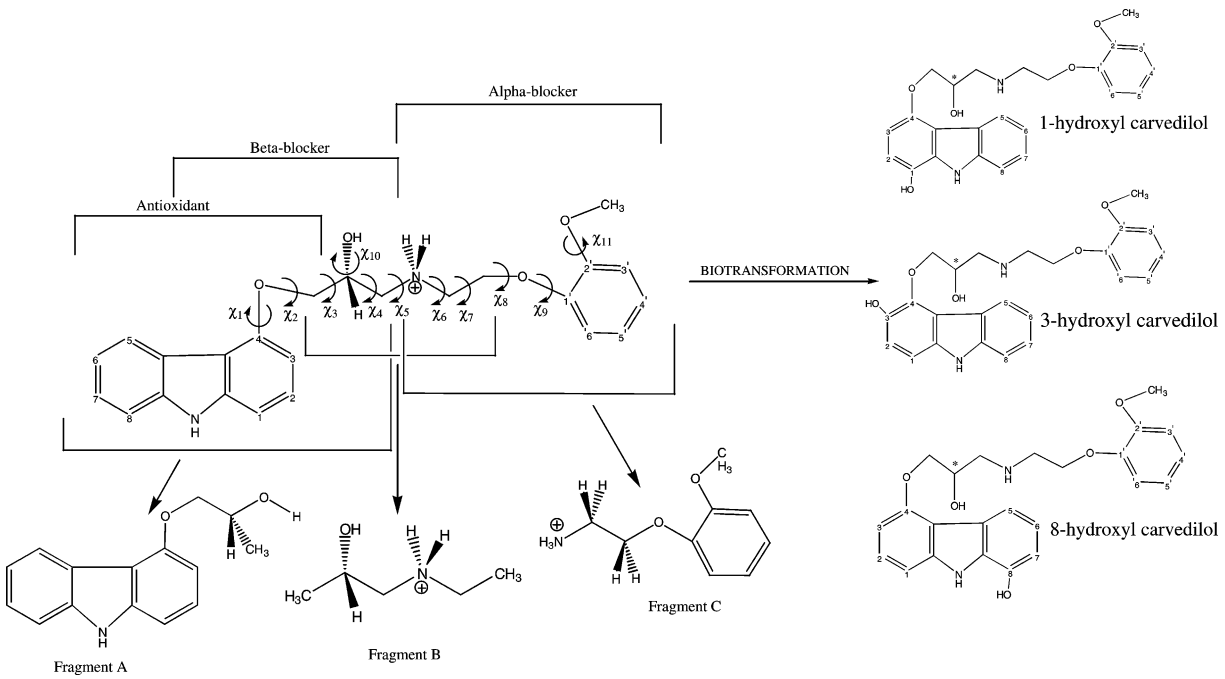

Fig. 1. The complete molecular structure and function of *N*-protonated carvedilol indicating all eleven torsional angles (top) and its three pharmocophoric fragments: *R*- and *S*-4-(2-hydroxypropoxy)carbazol (Fragment A), 2(*R* and *S*)-1-(ethylamonium)propane-2-ol (Fragment B), and aminoethoxy-2-methoxy-benzene (Fragment C). Upon biotransformation, three hydroxylated metabolites of carvedilol still possessing activity are formed: 1-hydroxyl, 3-hydroxyl, and 8-hydroxyl carvedilol (right).

the Fragment B stereocentre (c.f. Fig. 2).

$$E = f(\chi_4, \chi_5, \chi_6, \chi_{10}) \quad (1)$$

The structure of Fragment B indicates that carvedilol can be deprotonated via two protons. The latter is evident when either of the two protons is replaced by deuterium which leads to a nitrogen centre with either an *S*- or *R*-configuration, depending on which proton is replaced with deuterium. The protons are denoted as H_S (H16) and H_R (H21) in Fig. 2. This designation

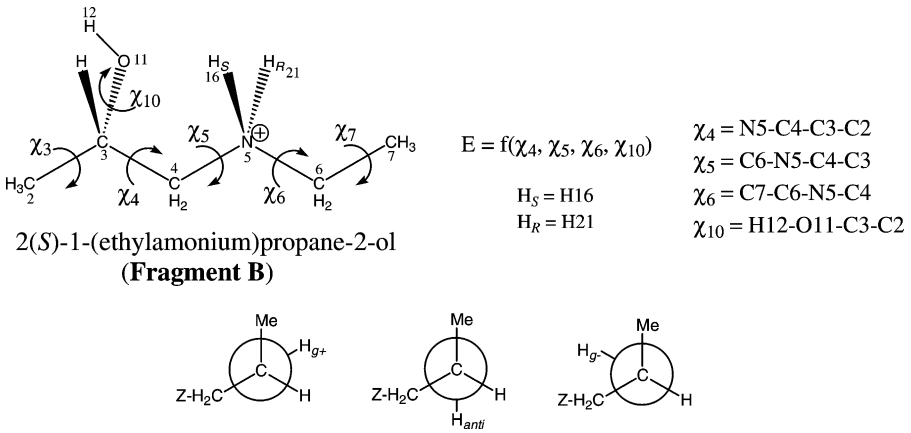

Fig. 2. Numbering and definition of torsional angles for 2(*S*)-1-(ethylamonium)propane-2-ol (Fragment B) (top). Newman projections along the C3-O11 bond (C3 front and O11 rear) display the g^+ (left), *anti* (middle), and g^- (right) conformations of torsional angle χ_{10} at the stereocentre of Fragment B and carvedilol. (Numbers placed beside atoms indicates numbering used as *z*-matrix input for GAUSSIAN 98.)

may also be applied to deprotonation scheme; for example, deprotonation of H_S would leave the nitrogen centre with H_R bonded and possessing an *R*-configuration. Therefore, dependent on the conformations adopted by Fragment B (and carvedilol accordingly), H_S and H_R will require different energies of deprotonation. Previous proton affinity studies on carvedilol and the amino group do not discriminate the different protons and reveal energies of deprotonation between 234 and 238 kcal mol^{-1} [11]. Multi-dimensional conformational analysis (MDCA) was performed on Fragment B to analyze the different energies of deprotonation associated with its full conformational space.

It is expected that, as it was shown for Fragment A, Fragment B will exhibit axis chirality as well as point chirality (from the *R*- and *S*-configurations) [20]. As such, the conformers present in the *R*-configuration PEHS can be predicted from the computed *S*-configuration of Fragment B according to Eq. (2). Eq. (2) states that stereoisomers, *S* and *R*, posses both point chirality and axis chirality and are exactly enantiomeric. Thus, a true enantiomeric pair requires not only the switching of point chirality from the *R*- to *S*-stereoisomer, but also the switching of all torsional angles from clockwise (CW) to counter-clockwise (CCW) rotation as demanded by Eq. (2). Consequently, the PEHS minima must all have an energetically equal enantiomer while all other pairs have diastereomeric relationships.

$$E_S = E_R \tag{2}$$

$$f_S(\chi_4, \chi_5, \chi_6, \chi_{10}) = f_R(-\chi_4, -\chi_5, -\chi_6, -\chi_{10}).$$

All computations were performed using the GAUSSIAN 98 software program [21]. Fragment B was exclusively defined using the GAUSSIAN 98 *z*-matrix internal coordinate system, to specify molecular structure, stereochemistry, and geometry. All calculations were performed at the Hartree–Fock, RHF/3-21G, level of theory.

Structural analysis of Fragment B was computed by MDCA of the Fragment B PEHS with optimizations of the conformational minima. With four torsional angles (χ_4, χ_5, χ_6, χ_{10}), and three possible minima for each torsional angle (*gauche plus*, g^+; *anti*, *a*; *gauche minus*, g^-), there are expected a grand total of 81 ($=3^4$) possible minima for each configuration of Fragment B. Only the *S*-configuration was computed because all structures are expected to be enantiomeric according to Eq. (2). Potential energy curves (PECs) were composed of either 12 or 24 points computed at 30° and 15° increments, respectively, according to Eq. (3) at the RHF/3-21G level of theory and plotted using Axum 5.0.

$$E = f(\chi_{10}) \tag{3}$$

After the PEHS was calculated, a separate two prong conformational methodology was applied to analyze the intrinsic basicity of the amino group of Fragment B. For each unique converged conformation of the PEHS, protonated Fragment B (BH^+) was deprotonated of protons H_S and H_R, independently of each other. Initially, vertical proton affinities were calculated with single-point energy (SPE) calculations and these energy values are denoted as $\Delta E_{vert}(S)$ and $\Delta E_{vert}(R)$ for H_S and H_R deprotonation, respectively (c.f. Eqs. (4) and (5)). The H_S and H_R deprotonated Fragment B (B) structures were then geometrically optimized and the respective adiabatic proton affinities (process in which the geometries are relaxed) were calculated based on fully optimized values. These values, denoted as $\Delta E_{opt}(S)$ and $\Delta E_{opt}(R)$ represent H_S and H_R optimized energies of deprotonation, respectively (c.f. Eqs. (6) and (7)). A third value, denoted as $\Delta\Delta E(S)$ and $\Delta\Delta E(R)$, represents the difference between the SPE [$\Delta E_{vert}(S)$ and $\Delta E_{vert}(R)$] and the optimized [$\Delta E_{opt}(S)$ and $\Delta E_{opt}(R)$] values for the energies of deprotonation for each conformer (c.f. Eqs. (8) and (9)]. This latter set of values can be interpreted as the stabilization experienced by Fragment B conformers as they adopted an optimized conformation after deprotonation. The above methodology is illustrated in Fig. 3. (A positive value for the energy of deprotonation appears because bond-breaking is always an endothermic process.)

$$\Delta E_{vert}(S) = |E_{opt}[BH^+] - E_{SP}[B]| \tag{4}$$

(H_S deprotonation)

$$\Delta E_{vert}(R) = |E_{opt}[BH^+] - E_{SP}[B]| \tag{5}$$

(H_R deprotonation)

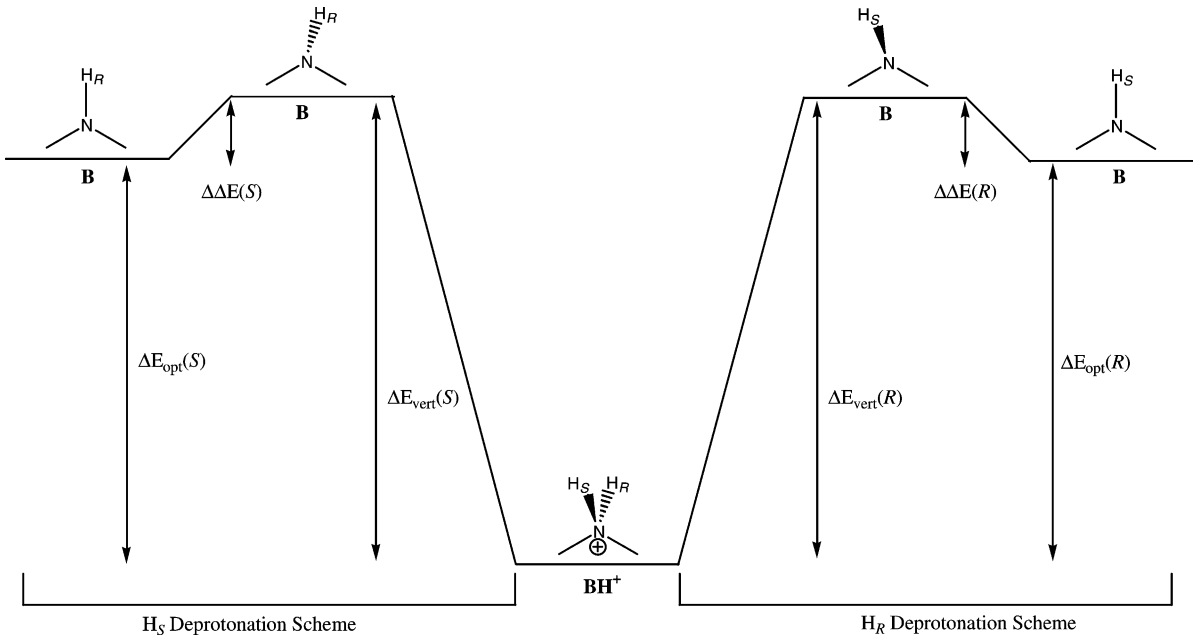

Fig. 3. Methodology employed to analyze the basicity of the amino group of Fragment B. Each converged minima of the protonated Fragment B PEHS was subject to independent deprotonation of the H_S (H16) and H_R (H21) protons (see Computational Method for explanation).

$$\Delta E_{\text{opt}}(S) = |E_{\text{opt}}[\text{BH}^+] - E_{\text{opt}}[\text{B}]| \quad (6)$$

(H_S deprotonation)

$$\Delta E_{\text{opt}}(R) = |E_{\text{opt}}[\text{BH}^+] - E_{\text{opt}}[\text{B}]| \quad (7)$$

(H_R deprotonation)

$$\Delta\Delta E(S) = \Delta E_{\text{vert}}(S) - \Delta E_{\text{opt}}(S) \quad (8)$$

(H_S deprotonation)

$$\Delta\Delta E(R) = \Delta E_{\text{vert}}(R) - \Delta E_{\text{opt}}(R) \quad (9)$$

(H_R deprotonation)

3. Results and discussion

3.1. MDCA and basicity of 2(S)-1-(ethylamonium)propane-2-ol (Fragment B)

The full PEHS of protonated Fragment B was investigated by geometry optimizations of the minima. All structures that converged were deprotonated of H_S and H_R, independently of each other, and then subject to further geometry optimizations. A full glossary (c.f. Table 1) and graphical representation (c.f. Fig. 4) of all converged protonated, H_S deprotonated, and H_R deprotonated minima is presented. Structural assignments for the conformational minima were made according to the conditions in Eq. (10).

gauche plus (g^+) = 60 (ideal) ± 60°

anti (a) = 180 (ideal) ± 60° (10)

gauche minus (g^-) = −60 (ideal) ± 60°.

This is based on the general observation that, if one were to rotate a tetrahedral carbon against another tetrahedral carbon, the minima would generally fall within the above ranges.

A total of 18 minima converged out of a possible 81 (22.2%) for the protonated PEHS of Fragment B (c.f. Table 2). As is clearly evident from the distribution of minima in Fig. 4, the dominant characteristic of all converged minima (protonated and deprotonated) was that all contained torsional angle χ_{10} (hydroxyl stereocentre) in the g^+ position. This was favoured because it

Table 1
Summary of converged conformational minima for the PEHS of 2(*S*)-1-(ethylamonium)propane-2-ol (Fragment B) at the RHF/3-21G level of theory for protonated (A), H_S (H16) deprotonated (B), and H_R (H21) deprotonated conformers (C) (F, Found; NF, Not Found; GM, Global Minima)

Conformational assignment				A	B	C	Conformational assignment				A	B	C	Conformational assignment				A	B	C
χ_4	χ_5	χ_6	χ_{10}				χ_4	χ_5	χ_6	χ_{10}				χ_4	χ_5	χ_6	χ_{10}			
g^+	g^+	g^+	g^+	F	F	F	*a*	g^+	g^+	g^+	F	NF	F	g^-	g^+	g^+	g^+	NF	NF	NF
g^+	g^+	g^+	*a*	NF	NF	NF	*a*	g^+	g^+	*a*	NF	NF	NF	g^-	g^+	g^+	*a*	NF	NF	NF
g^+	g^+	g^+	g^-	NF	NF	NF	*a*	g^+	g^+	g^-	NF	NF	NF	g^-	g^+	g^+	g^-	NF	NF	NF
g^+	g^+	*a*	g^+	NF	F	NF	*a*	g^+	*a*	g^+	F	NF	F	g^-	g^+	*a*	g^+	NF	NF	NF
g^+	g^+	*a*	*a*	NF	NF	NF	*a*	g^+	*a*	*a*	NF	NF	NF	g^-	g^+	*a*	*a*	NF	NF	NF
g^+	g^+	*a*	g^-	NF	NF	NF	*a*	g^+	*a*	g^-	NF	NF	NF	g^-	g^+	*a*	g^-	NF	NF	NF
g^+	g^+	g^-	g^+	NF	F	NF	*a*	g^+	g^-	g^+	F	NF	F	g^-	g^+	g^-	g^+	NF	NF	NF
g^+	g^+	g^-	*a*	NF	NF	NF	*a*	g^+	g^-	*a*	NF	NF	NF	g^-	g^+	g^-	*a*	NF	NF	NF
g^+	g^+	g^-	g^-	NF	NF	NF	*a*	g^+	g^-	g^-	NF	NF	NF	g^-	g^+	g^-	g^-	NF	NF	NF
g^+	*a*	g^+	g^+	F	NF	NF	*a*	*a*	g^+	g^+	F	F	F	g^-	*a*	g^+	g^+	F	F	NF
g^+	*a*	g^+	*a*	NF	NF	NF	*a*	*a*	g^+	*a*	NF	NF	NF	g^-	*a*	g^+	*a*	NF	NF	NF
g^+	*a*	g^+	g^-	NF	NF	NF	*a*	*a*	g^+	g^-	NF	NF	NF	g^-	*a*	g^+	g^-	NF	NF	NF
g^+	*a*	*a*	g^+	F	NF	F_{GM}	*a*	*a*	*a*	g^+	F_{GM}	F_{GM}	F	g^-	*a*	*a*	g^+	F	F	F
g^+	*a*	*a*	*a*	NF	NF	NF	*a*	*a*	*a*	*a*	NF	NF	NF	g^-	*a*	*a*	*a*	NF	NF	NF
g^+	*a*	*a*	g^-	NF	NF	NF	*a*	*a*	*a*	g^-	NF	NF	NF	g^-	*a*	*a*	g^-	NF	NF	NF
g^+	*a*	g^-	g^+	F	NF	F	*a*	*a*	g^-	g^+	F	F	NF	g^-	*a*	g^-	g^+	F	F	F
g^+	*a*	g^-	*a*	NF	NF	NF	*a*	*a*	g^-	*a*	NF	NF	NF	g^-	*a*	g^-	*a*	NF	NF	NF
g^+	*a*	g^-	g^-	NF	NF	NF	*a*	*a*	g^-	g^-	NF	NF	NF	g^-	*a*	g^-	g^-	NF	NF	NF
g^+	g^-	g^+	g^+	NF	NF	NF	*a*	g^-	g^+	g^+	NF	NF	NF	g^-	g^-	g^+	g^+	NF	NF	F
g^+	g^-	g^+	*a*	NF	NF	NF	*a*	g^-	g^+	*a*	NF	NF	NF	g^-	g^-	g^+	*a*	NF	NF	NF
g^+	g^-	g^+	g^-	NF	NF	NF	*a*	g^-	g^+	g^-	NF	NF	NF	g^-	g^-	g^+	g^-	NF	NF	NF
g^+	g^-	*a*	g^+	F	F	NF	*a*	g^-	*a*	g^+	NF	NF	NF	g^-	g^-	*a*	g^+	F	F	F
g^+	g^-	*a*	*a*	NF	NF	NF	*a*	g^-	*a*	*a*	NF	NF	NF	g^-	g^-	*a*	*a*	NF	NF	NF
g^+	g^-	*a*	g^-	NF	NF	NF	*a*	g^-	*a*	g^-	NF	NF	NF	g^-	g^-	*a*	g^-	NF	NF	NF
g^+	g^-	g^-	g^+	F	F	NF	*a*	g^-	g^-	g^+	F	F	F	g^-	g^-	g^-	g^+	F	F	F
g^+	g^-	g^-	*a*	NF	NF	NF	*a*	g^-	g^-	*a*	NF	NF	NF	g^-	g^-	g^-	*a*	NF	NF	NF
g^+	g^-	g^-	g^-	NF	NF	NF	*a*	g^-	g^-	g^-	NF	NF	NF	g^-	g^-	g^-	g^-	NF	NF	NF

allows the lone pairs of the oxygen atom (O11) to act as hydrogen bond acceptors towards the nitrogen proton(s). As such, conformers were stabilized by internal hydrogen bonds between O11 and either the H_S or H_R proton. The significance of this intramolecular hydrogen bonding is evident in the relative energies of the protonated conformers; all conformers with hydrogen bonding possesses relative energies below 4 kcal mol^{-1} while protonated conformers that lack the internal hydrogen bonding have relative energies between 6 and 13 kcal mol^{-1}. The hydrogen bond results in the formation of a five-membered ring as seen for the global minima of the protonated PEHS, $aaag^+$ (c.f. Fig. 5). Further, as indicated by the Newman projections in Fig. 2, the smallest steric hindrance occurs when the stereocentre χ_{10} is in the g^+ conformation, therefore, this stabilizing force adds to the prevalence of the g^+ conformation for torsional angle χ_{10}. The structural features of all converged protonated conformers are found in Table 3, Section 1.

Once the protonated PEHS of Fragment B was computed, the H_S and H_R protons were deprotonated as shown in Fig. 3. Upon deprotonation, SPE calculations were performed for each type of proton for each converged conformer and the non-optimized energy of deprotonation calculated (c.f. $\Delta E_{vert}(S)$ and $\Delta E_{vert}(R)$ in Table 2). It was found that conformers

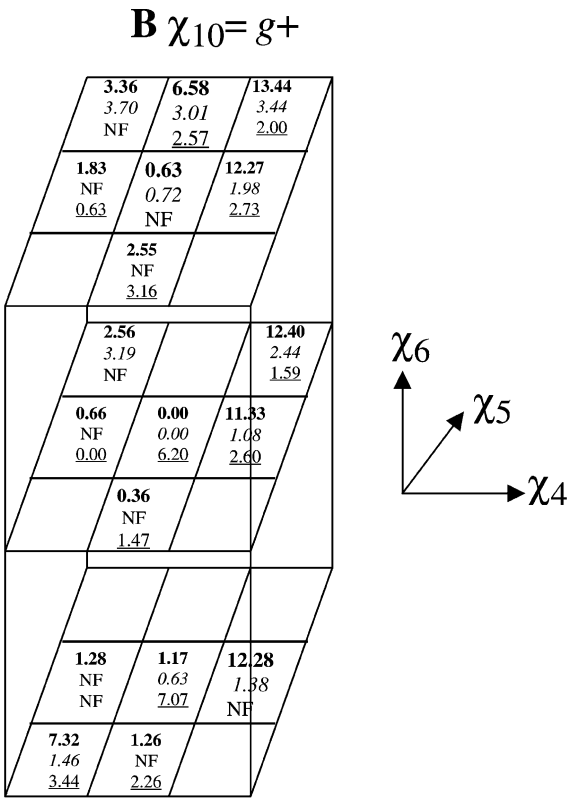

Fig. 4. Graphical summary of all converged conformational minima for the PEHS of 2(*S*)-1-(ethylamonium)propane-2-ol (Fragment B) at the RHF/3-21G level of theory. Relative energies are indicated as follows: bold values for converged protonated conformers, *italicized values* for converged H_S (H16) deprotonated conformers, and *underlined values* for converged H_R (H21) deprotonated conformers. Conformers which were not originally or subsequently found within a respective conformational assignment where at least one other minima converged are indicated with NF (Not Found). Blank spaces indicate conformational assignments that lacked any converged conformers. Note that all converged conformational minima possessed torsional angle χ_{10} in the g^+ conformation.

showed the greatest difference in the $\Delta E_{vert}(S)$ and $\Delta E_{vert}(R)$ energies of deprotonation when the conformers possessed hydrogen bonding between O11 with either of these two protons. In these instances, the proton not involved in hydrogen bonding was relatively easily deprotonated. However, the proton involved in hydrogen bonding possessed a larger energy of deprotonation because of its involvement in intramolecular stabilization. The latter trend was present for all protonated conformers possessing internal hydrogen bonding (c.f. 3.2 relative basicity of the H_S and H_R protons below).

After all non-optimized energies of deprotonation had been calculated, all H_S (c.f. Table 4) and H_R (c.f. Table 5) deprotonated conformers were subject to full geometry optimizations. Not every unique protonated conformed converged to a unique deprotonated conformer upon optimization (i.e. some deprotonated conformers converged to the same molecular conformation upon optimization). Of the H_S deprotonated conformers (c.f. Table 4), the global minima $aaag^+$ retained the intramolecular hydrogen bond, albeit a longer and weaker hydrogen bond (2.28 Å), between O11 and H_R found in the protonated global minima having the same conformation (c.f. Fig. 5). Of the H_R deprotonated conformers (c.f. Table 5), the global minima was found to be g^+aag^+. This conformer possessed a five-membered ring with a 2.27 Å hydrogen bond very similar to the H_S deprotonated global minima. Structural features of converged H_S and H_R deprotonated conformers are found in Table 3, Sections 2 and 3, respectively.

With regards to the structural features present in the deprotonated conformers, hydrogen bonding was not as dominant a stabilization force as that found for the protonated conformers. This was due to the fact that the lone pair now exposed on the nitrogen atom repelled the hydrogen bond donor lone pairs of O11. When the nitrogen was protonated and positively charged, an ion–dipole interaction was present between the nitrogen and oxygen atoms. Upon deprotonation, this interaction was removed. The repulsion experienced between the two heteroatoms is evident based on the much longer hydrogen bond distances in the optimized deprotonated conformers.

All deprotonated conformers, like the protonated PEHS conformers, possessed torsional angle χ_{10} in the g^+ position. To further investigate the persistence of this *gauche effect* on the conformational identity of Fragment B, PECs were computed according to Eq. (3). For both protonated and deprotonated Fragment B, PECs were generated with torsional angles χ_4, χ_5, and χ_6 in the *anti* position; however, for completeness, one PEC was generated with χ_4, χ_5, and χ_6 at optimized *anti* values (based on the $aaag^+$ conformation) and one PEC was generated with these three torsional angles frozen in the *anti* position at 180.00° (c.f. Fig. 6).

Table 2
Optimized minima for the PEHS of 2(*S*)-1-(ethylamonium)propane-2-ol (Fragment B) computed at the RHF/3-21G level of theory. Optimizations were followed by SPE calculations for independent deprotonation of H_S (H16) and H_R (H21) protons, denoted as $\Delta E_{vert}(S)$ and $\Delta E_{vert}(R)$, respectively

Conformational assignment				χ_4 degrees	χ_5 degrees	χ_6 degrees	χ_{10} degrees	*E* (hartree) protonated; deprotonated H_S; deprotonated H_R	Relative *E*; $\Delta E_{vert}(S)$; $\Delta E_{vert}(R)$ (kcal mol^{-1})
χ_4	χ_5	χ_6	χ_{10}						
g^+	g^+	g^+	g^+	57.38	66.37	58.14	70.70	−324.793727316; −324.383143312; −324.381925633	7.32; 257.65; 258.41
g^+	g^+	g^+	a					NOT FOUND MOVED TO $g^+ag^+g^+$	
g^+	g^+	g^+	g^-					NOT FOUND MOVED TO $g^+g^+g^+g^+$	
g^+	g^+	a	g^+					NOT FOUND MOVED TO g^+aag^+	
g^+	g^+	a	a					NOT FOUND MOVED TO g^+aag^+	
g^+	g^+	a	g^-					NOT FOUND MOVED TO g^+aag^+	
g^+	g^+	g^-	g^+					NOT FOUND MOVED TO g^+aag^+	
g^+	g^+	g^-	a					NOT FOUND MOVED TO g^+aag^+	
g^+	g^+	g^-	g^-					NOT FOUND MOVED TO $g^+ag^-g^+$	
g^+	a	g^+	g^+	77.45	155.53	66.95	66.96	−324.803348723; −324.370422703; −324.382241913	1.28; 271.67; 264.25
g^+	a	g^+	a					NOT FOUND MOVED TO $g^+ag^+g^+$	
g^+	a	g^+	g^-					NOT FOUND MOVED TO $g^+ag^+g^+$	
g^+	a	a	g^+	77.04	157.33	−179.56	67.45	−324.804338872; −324.370793410; −324.383547600	0.66; 272.05; 264.05
g^+	a	a	a					NOT FOUND MOVED TO g^+aag^+	
g^+	a	a	g^-					NOT FOUND MOVED TO g^+aag^+	
g^+	a	g^-	g^+	77.04	158.06	−75.46	67.12	−324.802468298; −324.369387191; −324.382362342	1.83; 271.76; 263.62
g^+	a	g^-	a					NOT FOUND MOVED TO $g^+ag^-g^+$	
g^+	a	g^-	g^-					NOT FOUND MOVED TO $g^+ag^-g^+$	
g^+	g^-	g^+	g^+					NOT FOUND MOVED TO aag^+g^+	
g^+	g^-	g^+	a					NOT FOUND MOVED TO aag^+g^+	
g^+	g^-	g^+	g^-					NOT FOUND MOVED TO aag^+g^+	
g^+	g^-	a	g^+	89.94	−98.15	179.17	65.87	−324.801304451; −324.376716678; −324.365840488	2.56; 266.43; 273.26
g^+	g^-	a	a					NOT FOUND MOVED TO $g^+g^-ag^+$	
g^+	g^-	a	g^-					NOT FOUND MOVED TO $g^+g^-ag^+$	
g^+	g^-	g^-	g^+	88.01	−100.37	−75.18	65.30	−324.800033440; −324.375899954; −324.365661207	3.36; 266.15; 272.57
g^+	g^-	g^-	a					NOT FOUND MOVED TO $g^+g^-g^-g^+$	
g^+	g^-	g^-	g^-					NOT FOUND MOVED TO $g^+g^-g^-g^+$	
a	g^+	g^+	g^+	160.44	84.73	75.97	51.78	−324.803380654; −324.370295100; −324.380697015	1.26; 271.77; 265.24
a	g^+	g^+	a					NOT FOUND MOVED TO $ag^+g^+g^+$	
a	g^+	g^+	g^-					NOT FOUND MOVED TO $ag^+g^+g^+$	
a	g^+	a	g^+	159.67	82.59	−178.21	50.43	−324.804820840; −324.371180064; −324.382020238	0.36; 272.11; 265.31
a	g^+	a	a					NOT FOUND MOVED TO ag^+ag^+	
a	g^+	a	g^-					NOT FOUND MOVED TO ag^+ag^+	
a	g^+	g^-	g^+	151.31	95.77	−64.00	50.51	−324.801332654; −324.366403815; −324.378430764	2.55; 272.92; 265.37
a	g^+	g^-	a					NOT FOUND MOVED TO $ag^+g^-g^+$	
a	g^+	g^-	g^-					NOT FOUND MOVED TO $ag^+g^-g^+$	

(*continued on next page*)

Table 2 (*continued*)

Conformational assignment				χ_4 degrees	χ_5 degrees	χ_6 degrees	χ_{10} degrees	E (hartree) protonated; deprotonated H_S; deprotonated H_R	Relative E; $\Delta E_{vert}(S)$; $\Delta E_{vert}(R)$ (kcal mol^{-1})
χ_4	χ_5	χ_6	χ_{10}						
a	*a*	g^+	g^+	163.82	−160.12	74.88	52.72	−324.803518745; −324.382647073; −324.370596945	1.17; 264.10; 271.66
a	*a*	g^+	*a*					NOT FOUND MOVED TO aag^+g^+	
a	*a*	g^+	g^-					NOT FOUND MOVED TO aag^+g^+	
a	*a*	*a*	g^+	163.43	−158.84	179.48	52.99	−324.805389226; −324.383705631; −324.371916613	0.00; 264.61; 272.01
a	*a*	*a*	*a*					NOT FOUND MOVED TO $aaag^+$	
a	*a*	*a*	g^-					NOT FOUND MOVED TO $aaag^+$	
a	*a*	g^-	g^+	163.01	−157.12	−67.28	53.23	−324.804392810; −324.382419825; −324.371475806	0.63; 264.79; 271.66
a	*a*	g^-	*a*					NOT FOUND MOVED TO aag^-g^+	
a	*a*	g^-	g^-					NOT FOUND MOVED TO aag^-g^+	
a	g^-	g^+	g^+					NOT FOUND MOVED TO $aaag^+$	
a	g^-	g^+	*a*					NOT FOUND MOVED TO $aaag^+$	
a	g^-	g^+	g^-					NOT FOUND MOVED TO $aaag^+$	
a	g^-	*a*	g^+					NOT FOUND MOVED TO $aaag^+$	
a	g^-	*a*	*a*					NOT FOUND MOVED TO $aaag^+$	
a	g^-	*a*	g^-					NOT FOUND MOVED TO $aaag^+$	
a	g^-	g^-	g^+	−175.68	−67.90	−56.89	47.87	−324.794908573; −324.382377089; −324.382826135	6.58; 258.87; 258.59
a	g^-	g^-	*a*					NOT FOUND MOVED TO $ag^-g^-g^+$	
a	g^-	g^-	g^-					NOT FOUND MOVED TO aag^-g^+	
g^-	g^+	g^+	g^+					NOT FOUND MOVED TO $g^-ag^+g^+$	
g^-	g^+	g^+	*a*					NOT FOUND MOVED TO $g^-ag^+g^+$	
g^-	g^+	g^+	g^-					NOT FOUND MOVED TO $g^-ag^+g^+$	
g^-	g^+	*a*	g^+					NOT FOUND MOVED TO g^-aag^+	
g^-	g^+	*a*	*a*					NOT FOUND MOVED TO g^-aag^+	
g^-	g^+	*a*	g^-					NOT FOUND MOVED TO g^-aag^+	
g^-	g^+	g^-	g^+					NOT FOUND MOVED TO $g^-ag^-g^+$	
g^-	g^+	g^-	*a*					NOT FOUND MOVED TO g^-aag^+	
g^-	g^+	g^-	g^-					NOT FOUND MOVED TO $g^-ag^-g^+$	
g^-	*a*	g^+	g^+	−65.71	179.45	71.69	61.00	−324.785812572; −324.384528756; −324.382471731	12.28; 251.81; 253.10
g^-	*a*	g^+	*a*					NOT FOUND MOVED TO $g^-ag^+g^+$	
g^-	*a*	g^+	g^-					NOT FOUND MOVED TO $g^-ag^+g^+$	
g^-	*a*	*a*	g^+	−65.08	−178.48	−179.82	61.68	−324.787326426; −324.385190901; −324.384040306	11.33; 252.34; 253.07
g^-	*a*	*a*	*a*					NOT FOUND MOVED TO g^-aag^+	
g^-	*a*	*a*	g^-					NOT FOUND MOVED TO g^-aag^+	
g^-	*a*	g^-	g^+	−64.62	−175.20	−70.01	62.22	−324.785836750; −324.383589352; −324.383583730	12.27; 252.41; 252.42
g^-	*a*	g^-	*a*					NOT FOUND MOVED TO $g^-ag^-g^+$	
g^-	*a*	g^-	g^-					NOT FOUND MOVED TO $g^-ag^-g^+$	
g^-	g^-	g^+	g^+					NOT FOUND MOVED TO $g^-ag^+g^+$	
g^-	g^-	g^+	*a*					NOT FOUND MOVED TO $g^-ag^+g^+$	
g^-	g^-	g^+	g^-					NOT FOUND MOVED TO $g^-ag^+g^+$	

g^-	g^-	a	g^+	−60.25	−69.11	−175.71	65.39	−324.785622305; −324.383378864; −324.384106841	12.40; 252.41; 251.95
g^-	g^-	a	a					NOT FOUND MOVED TO $g^-g^-ag^+$	
g^-	g^-	a	g^-					NOT FOUND MOVED TO $g^-g^-ag^+$	
g^-	g^-	g^-	g^+	−60.25	−67.59	−67.79	64.38	−324.783970218; −324.381707969; −324.383073438	13.44; 252.42; 251.57
g^-	g^-	g^-	a					NOT FOUND MOVED TO $g^-g^-g^-g^+$	
g^-	g^-	g^-	g^-					NOT FOUND MOVED TO $g^-g^-g^-g^+$	

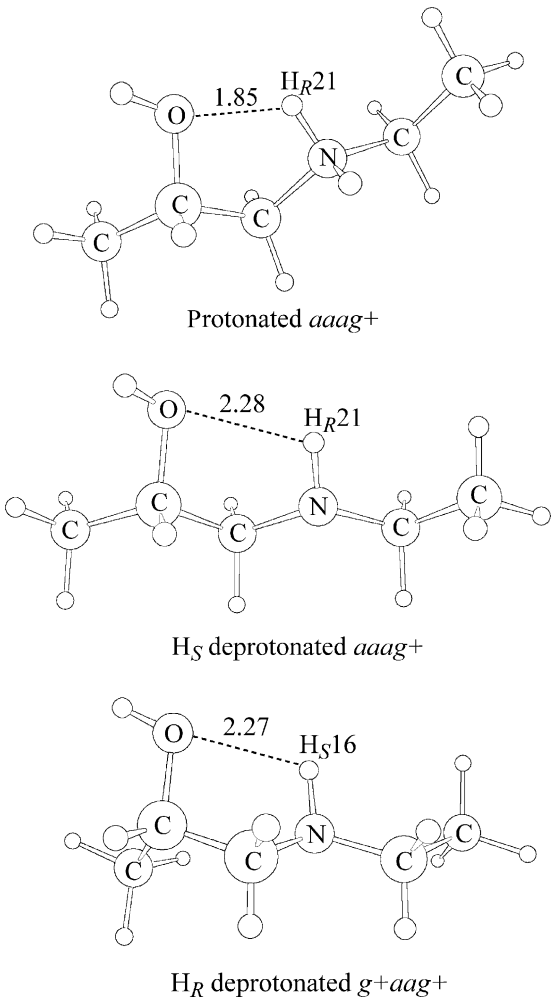

Fig. 5. Optimized global minima of the protonated Fragment B PEHS ($aaag^+$), H_S deprotonated Fragment B PEHS ($aaag^+$), and H_R deprotonated Fragment B PEHS (g^+aag^+).

For protonated Fragment B, one can see a profound *gauche effect* in both the χ_4-χ_5-χ_6-optimized and χ_4-χ_5-χ_6-frozen PECs. The χ_4-χ_5-χ_6-optimized PEC contains a deep minima about g^+, a very small minima at the *anti* conformation, and a very large barrier of rotation about the g^- position. The *gauche effect* is due to the hydrogen bonding prevalent in stable conformers between O11 and either nitrogen protons while the large barrier of rotation may be attributed to the repulsion between H12 and the positive nitrogen centre along with the steric hindrance between H12 and the Fragment B backbone. The *gauche effect* is exaggerated in

Table 3
Structural features of the converged protonated and deprotonated conformers of the 2(*S*)-1-(ethylamonium)propane-2-ol (Fragment B) PEHS. (All structures presented in this table were subject to full geometry optimizations at the RHF/3-21G level of theory)

Conformational assignment				#	Structural features	Relative E (kcal mol^{-1})
χ_4	χ_5	χ_6	χ_{10}			
I. Protonated conformers (BH^+)						
g^+	g^+	g^+	g^+	1	–	7.32
g^+	a	g^+	g^+	2	1.81 Å O11···H16 H-bond forming a 5-membered ring	1.28
g^+	a	a	g^+	3	1.83 Å O11···H16 H-bond forming a 5-membered ring	0.66
g^+	a	g^-	g^+	4	1.83 Å O11···H16 H-bond forming a 5-membered ring	1.83
g^+	g^-	a	g^+	5	1.74 Å O11···H21 H-bond forming a 5-membered ring	2.56
g^+	g^-	g^-	g^+	6	1.74 Å O11···H21 H-bond forming a 5-membered ring	3.36
a	g^+	g^+	g^+	7	1.80 Å O11···H16 H-bond forming a 5-membered ring	1.26
a	g^+	a	g^+	8	1.82 Å O11···H16 H-bond forming a 5-membered ring	0.36
a	g^+	g^-	g^+	9	1.75 Å O11···H16 H-bond forming a 5-membered ring	2.55
a	a	g^+	g^+	10	1.85 Å O11···H21 H-bond forming a 5-membered ring	1.17
a	a	a	g^+	11	1.85 Å O11···H21 H-bond forming a 5-membered ring	0.00
a	a	g^-	g^+	12	1.83 Å O11···H21 H-bond forming a 5-membered ring	0.63
a	g^-	g^-	g^+	13	–	6.58
g^-	a	g^+	g^+	14	–	12.28
g^-	a	a	g^+	15	–	11.33
g^-	a	g^-	g^+	16	–	12.27
g^-	g^-	a	g^+	17	–	12.4
g^-	g^-	g^-	g^+	18	–	13.44
II. H_S Deprotonated conformers (B)						
g^+	g^+	g^+	g^+		–	1.46
g^+	g^+	a	g^+		–	1.16
g^+	g^+	g^-	g^+		–	2.65
g^+	g^-	a	g^+		2.36 Å O11···H21 H-bond forming a 5-membered ring	3.19
g^+	g^-	g^-	g^+		2.32 Å O11···H21 H-bond forming a 5-membered ring	3.70
a	a	g^+	g^+		2.30 Å O11···H21 H-bond forming a 5-membered ring	0.63
a	a	a	g^+		2.28 Å O11···H21 H-bond forming a 5-membered ring	0.00
a	a	g^-	g^+		2.25 Å O11···H21 H-bond forming a 5-membered ring	0.72
a	g^-	g^-	g^+		–	3.01
g^-	a	g^+	g^+		–	1.38
g^-	a	a	g^+		–	1.08
g^-	a	g^-	g^+		–	1.98
g^-	g^-	a	g^+		–	2.44
g^-	g^-	g^-	g^+		–	3.44
III. H_R Deprotonated conformers (B)						
g^+	g^+	g^+	g^+		–	3.44
g^+	a	g^+	g^+		2.24 Å O11···H16 H-bond forming a 5-membered ring	0.74
g^+	a	a	g^+		2.27 Å O11…H16 H-bond forming a 5-membered ring	0.00
g^+	a	g^-	g^+		2.29 Å O11···H16 H-bond forming a 5-membered ring	0.63
a	g^+	g^+	g^+		2.36 Å O11···H16 H-bond forming a 5-membered ring	2.26
a	g^+	a	g^+		2.39 Å O11···H16 H-bond forming a 5-membered ring	1.47
a	g^+	g^-	g^+		2.34 Å O11···H16 H-bond forming a 5-membered ring	3.16
a	a	g^+	g^+		–	7.07
a	a	a	g^+		–	6.20
a	g^-	g^-	g^+		–	2.57
g^-	g^-	g^+	g^+		–	2.95
g^-	a	a	g^+		–	2.60
g^-	a	g^-	g^+		–	2.73
g^-	g^-	a	g^+		–	1.59
g$^-$	g$^-$	g$^-$	g$^+$		–	2.00

Table 4
Optimized conformational minima for the H_S (H16) deprotonated PEHS of 2(*S*)-1-(ethylamonium)propane-2-ol (Fragment B) at the RHF/3-21G level of theory

Optimized protonated conformation				Optimized deprotonated conformation				χ_4 degrees	χ_5 degrees	χ_6 degrees	χ_{10} degrees	*E* (hartree)	Relative *E* (kcal mol^{-1})	$\Delta E_{opt}(S)$ (kcal mol^{-1})	$\Delta\Delta E(S)$ (kcal mol^{-1})
χ_4	χ_5	χ_6	χ_{10}	χ_4	χ_5	χ_6	χ_{10}								
g^+	g^+	g^+	g^+	g^+	g^+	g^+	g^+	50.43	83.64	77.22	49.67	−324.394428616	1.46	250.56	7.09
g^+	*a*	g^+	g^+	g^+	g^+	g^+	g^+						1.46	256.60	15.07
g^+	*a*	*a*	g^+	g^+	g^+	*a*	g^+	50.95	84.16	−172.11	51.08	−324.394908988	1.16	256.92	15.13
g^+	*a*	g^-	g^+	g^+	g^+	g^-	g^+	56.57	83.85	−119.59	53.43	−324.392530627	2.65	257.24	14.52
g^+	g^-	*a*	g^+	g^+	g^-	*a*	g^+	64.42	−97.94	−165.27	56.27	−324.391676422	3.19	257.05	9.38
g^+	g^-	g^-	g^+	g^+	g^-	g^-	g^+	64.05	−104.16	−79.37	56.73	−324.390858084	3.70	256.76	9.39
a	g^+	g^+	g^+	*a*	*a*	g^+	g^+						0.63	255.78	15.99
a	g^+	*a*	g^+	*a*	*a*	*a*	g^+						0.00	256.06	16.05
a	g^+	g^-	g^+	*a*	*a*	g^-	g^+						0.72	254.60	18.32
a	*a*	g^+	g^+	*a*	*a*	g^+	g^+	−179.70	176.35	68.11	68.85	−324.395761426	0.63	255.87	8.23
a	*a*	*a*	g^+	*a*	*a*	*a*	g^+	179.76	−178.55	−178.61	68.55	−324.396758432	0.00	256.42	8.19
a	*a*	g^-	g^+	*a*	*a*	g^-	g^+	179.09	−176.55	−76.04	68.61	−324.395608581	0.72	256.52	8.27
a	g^-	g^-	g^+	*a*	g^-	g^-	g^+	−169.50	−62.51	−52.24	63.94	−324.391953903	3.01	252.86	6.01
g^-	*a*	g^+	g^+	g^-	*a*	g^+	g^+	−63.77	158.80	67.41	55.51	−324.394564704	1.38	245.51	6.30
g^-	*a*	*a*	g^+	g^-	*a*	*a*	g^+	−63.66	165.72	−176.33	55.45	−324.395037053	1.08	246.17	6.17
g^-	*a*	g^-	g^+	g^-	*a*	g^-	g^+	−63.79	165.45	−78.14	55.38	−324.393598336	1.98	246.13	6.28
g^-	g^-	*a*	g^+	g^-	g^-	*a*	g^+	−61.45	−67.54	−167.25	61.43	−324.392871990	2.44	246.45	5.96
g^-	g^-	g^-	g^+	g^-	g^-	g^-	g^+	−62.03	−70.31	−74.28	61.11	−324.391281427	3.44	246.42	6.00

Table 5
Optimized conformational minima for the H_R (H21) deprotonated PEHS of 2(*S*)-1-(ethylamonium)propane-2-ol (Fragment B) at the RHF/3-21G level of theory

Optimized protonated conformation				Optimized deprotonated conformation				χ_4 degrees	χ_5 degrees	χ_6 degrees	χ_{10} degrees	*E* (hartree)	Relative *E* (kcal mol^{-1})	$\Delta E_{opt}(R)$ (kcal mol^{-1})	$\Delta\Delta E(R)$ (kcal mol^{-1})
χ_4	χ_5	χ_6	χ_{10}	χ_4	χ_5	χ_6	χ_{10}								
g^+	g^+	g^+	g^+	g^+	g^+	g^+	g^+	51.28	62.71	57.55	56.22	−324.391921532	3.44	252.14	6.27
g^+	*a*	g^+	g^+	g^+	*a*	g^+	g^+	62.16	178.29	76.43	51.71	−324.396225633	0.74	255.47	8.78
g^+	*a*	*a*	g^+	g^+	*a*	*a*	g^+	61.53	−179.94	178.63	51.76	−324.397398012	0.00	255.36	8.69
g^+	*a*	g^-	g^+	g^+	*a*	g^-	g^+	61.10	−174.77	−67.91	51.53	−324.396390104	0.63	254.82	8.80
g^+	g^-	*a*	g^+	g^+	*a*	*a*	g^+						0.00	253.46	19.80
g^+	g^-	g^-	g^+	g^+	*a*	g^-	g^+						0.63	253.29	19.28
a	g^+	g^+	g^+	*a*	g^+	g^+	g^+	176.20	79.56	79.77	63.77	−324.393799336	2.26	257.02	8.22
a	g^+	*a*	g^+	*a*	g^+	*a*	g^+	175.64	75.73	174.34	63.35	−324.395057646	1.47	257.13	8.18
a	g^+	g^-	g^+	*a*	g^+	g^-	g^+	173.28	94.91	−71.86	63.65	−324.392355344	3.16	256.64	8.73
a	*a*	g^+	g^+	*a*	*a*	g^+	g^+	−166.91	−164.54	77.40	70.40	−324.386129069	7.07	261.92	9.74
a	*a*	*a*	g^+	*a*	*a*	*a*	g^+	−167.45	−165.09	175.81	70.54	−324.387523460	6.20	262.21	9.8
a	*a*	g^-	g^+	*a*	g^-	g^-	g^+						2.57	257.96	13.7
a	g^-	g^-	g^+	*a*	g^-	g^-	g^+	−168.04	−82.94	−77.07	70.83	−324.393306541	2.57	252.01	6.58
g^-	*a*	g^+	g^+	g^-	g^-	g^+	g^+	−61.38	−110.00	73.08	57.70	−324.392689804	2.95	246.69	6.41
g^-	*a*	*a*	g^+	g^-	*a*	*a*	g^+	−64.05	−156.73	176.23	60.89	−324.393253702	2.60	247.28	5.79
g^-	*a*	g^-	g^+	g^-	*a*	g^-	g^+	−63.12	−144.51	−68.17	60.18	−324.393040514	2.73	246.48	5.94
g^-	g^-	*a*	g^+	g^-	g^-	*a*	g^+	−62.99	−86.60	176.93	56.92	−324.394864360	1.59	245.20	6.75
g^-	g^-	g^-	g^+	g^-	g^-	g^-	g^+	−63.66	−89.52	−75.03	56.64	−324.394212001	2.00	244.58	6.99

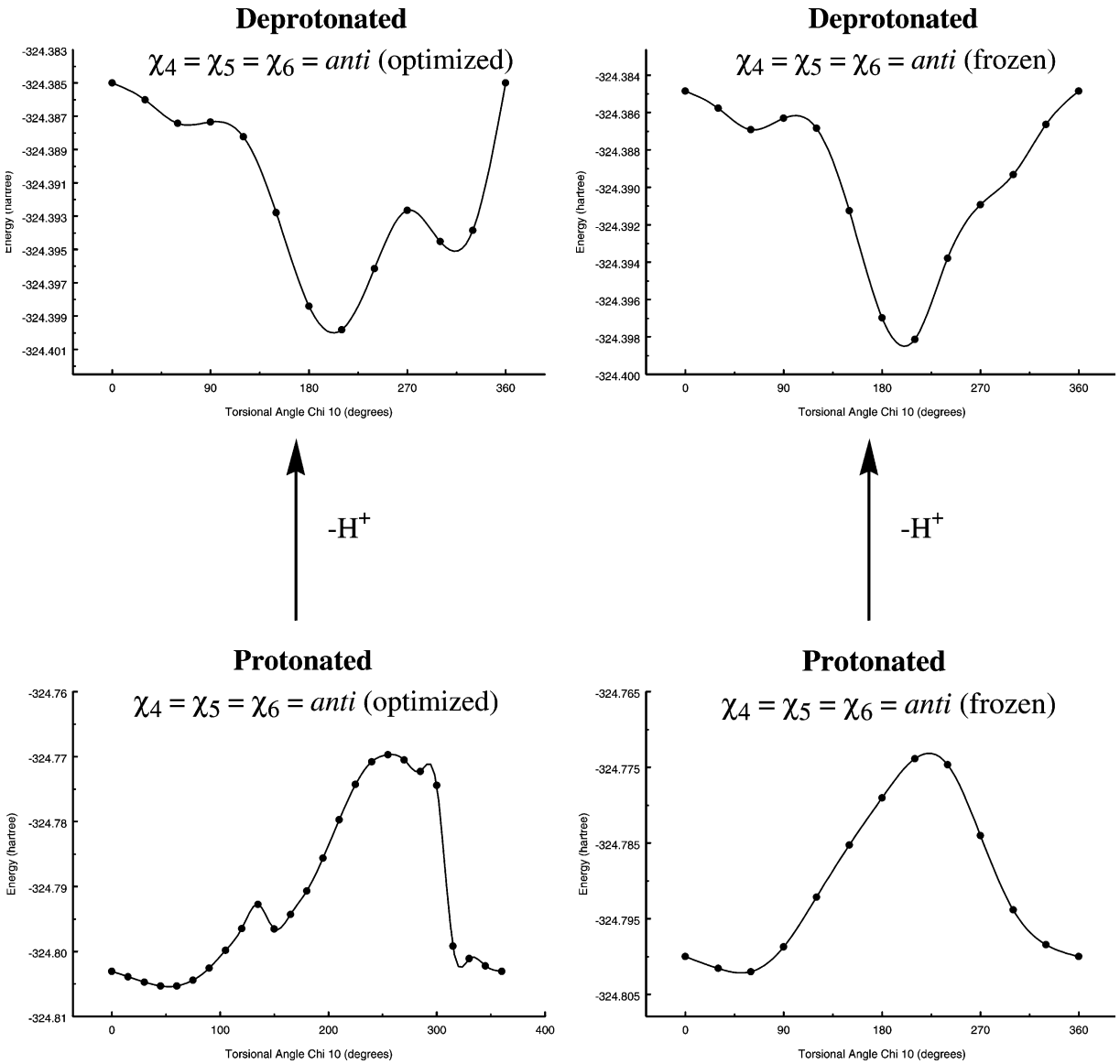

Fig. 6. PECs of torsional angle χ_{10} computed at the RHF/3-21G level of theory. PECs of protonated and deprotonated Fragment B with χ_4, χ_5, and χ_6 optimized and frozen in the *anti* conformation are shown.

the χ_4-χ_5-χ_6-frozen PEC, which lacks the subtle *anti* minima. This amplified *gauche effect* may be attributed to the inability of the H12, H_S, H_R, and $-CH_2-Z$ groups to avoid each other during the g^- rotation due to the freezing of the χ_4, χ_5, and χ_6 torsional angles.

Although only 22% of the possible protonated PEHS minima converged, this value may be revised in light of the *gauche effect* seen at the g^+ position for torsional angle χ_{10}. When one considers only the 27 conformational minima where χ_{10} is in the g^+ position, then 66.7% of conformers converged and were found for the protonated PEHS. Contrasting, zero minima converged for conformational assignments where torsional angle χ_{10} was either in

the *anti* or g^- position. This illustrates the dominant *gauche effect* in the conformational identity of Fragment B.

With regards to deprotonated Fragment B, a very different topological behaviour is depicted in the generated PECs (c.f. Fig. 6). The χ_4-χ_5-χ_6-optimized PEC possesses an *anti effect* and the significant g^+ *gauche effect* has been almost completely abolished and the large barrier of rotation in the g^- position has been replaced by a local minima. The χ_4-χ_5-χ_6-frozen PEC illustrates the same *anti effect*, however, the g^- local minima is absent from the PEC. The *anti effect* arises from the probable hydrogen bonding between H12 and the nitrogen lone pair when χ_{10} is in the *anti* position. The *anti* position also allows for hydrogen bonding between either nitrogen proton and O11.

Interestingly, although the PECs show this *anti effect*, it is completely absent from the geometrical optimizations of the deprotonated Fragment B minima (c.f. Table 4 and 5). This may be due in part to torsional angles χ_4, χ_5, and χ_6, which have a greater effect on the overall conformation than is evident from the PECs. Also, prevalence of the χ_{10} torsional angle in the g^+ conformation in protonated PEHS conformers (due to the *gauche effect* in the protonated structure), may largely determine the conformation that torsional angle χ_{10} assumes in the deprotonated state. This is said because hydrogen bonding alone is not deterministic of the g^+ conformation; the barrier of rotation (as indicated by the Newman projections) must also be taken into account. In other words, although hydrogen bonding seems to act as the dominant intramolecular stabilization force (as exemplified by the relative energies of hydrogen bonded conformers versus conformers that lack internal hydrogen bonding), it is not only in hydrogen bonded conformers that torsional angle χ_{10} adopts the g^+ conformation. Instead, all protonated and deprotonated conformers that do not possess internal hydrogen bonding still have the χ_{10} torsional angle oriented in the g^+ position. The latter further emphasizes the significance of the barrier of rotation that is deterministic of the conformational character of Fragment B and carvedilol's backbone. Therefore, the *gauche effect* in protonated Fragment B may influence the conformational identity of deprotonated Fragment B such that the *gauche effect* is still seen on the geometrically optimized minima of the deprotonated structures, although the PECs display an *anti effect* for torsional angle χ_{10}.

3.2. Relative basicity of the H_S and H_R protons

Carvedilol, with a pK_a of 7.9, is expected to be involved in a large number of protonophoretic pathways. At a physiological pH of 7.4, about two-thirds of the amino group is in its protonated form. To further study the basicity of the amino group, the relative basicity of the different protons, H_S and H_R, was investigated.

Initially, non-optimized energies of deprotonation ($\Delta E_{vert}(S)$ and $\Delta E_{vert}(R)$) revealed that conformers were subject to variable deprotonation energies dependent on whether or not one of the protons was involved in internal hydrogen bonding (c.f. Table 2). Upon comparing the differences in $\Delta E_{vert}(S)$ and $\Delta E_{vert}(R)$, it was found that conformers with no hydrogen bonding contained comparable energies of deprotonation for H_S and H_R, usually less that than 1 kcal mol^{-1} difference between the two protons (c.f. $|\Delta E_{vert}(S) - \Delta E_{vert}(R)|$ in Table 6). However, for conformers with internal hydrogen bonding, the hydrogen bonded proton usually required an additional 6–8 kcal mol^{-1} for deprotonation (c.f. Table 6). The latter trends are displayed in Fig. 7 (top) indicating that conformers with internal hydrogen bonding varied in $\Delta E_{vert}(S)$ and $\Delta E_{vert}(R)$ values, depending on which proton was involved in hydrogen bonding. However, conformers with no internal hydrogen bonding present displayed no such differences in their respective $\Delta E_{vert}(S)$ and $\Delta E_{vert}(R)$ energies of deprotonation since either proton could be abstracted with roughly the same investment of energy.

Upon optimization of deprotonated conformers, optimized energies of deprotonation were calculated for each H_S and H_R deprotonated conformer in Table 4 and 5, respectively, and in Table 6. As expected, geometry optimizations of the deprotonated conformers reduced the majority of differences between the H_S and H_R protons found in the non-optimized energies of deprotonation (c.f. Table 6). However, for the conformers aag^+g^+ and $aaag^+$, the H_R proton required an addition 6.05 and 5.79 kcal mol^{-1}, respectively, for deprotonation compared to the H_S proton (c.f. Fig. 7, middle). In

Table 6
Summary of energies of deprotonation and the differences found between H_S (H16) and H_R (H21) deprotonation for each converged conformation of 2(*S*)-1-(ethylamonium)propane-2-ol (Fragment B) at the RHF/3-21G level of theory

Protonated conformation				$\Delta E_{vert}(S)$ (kcal mol^{-1})	$\Delta E_{vert}(R)$ (kcal mol^{-1})	$\lvert\Delta E_{vert}(S) - \Delta E_{vert}(R)\rvert$ (kcal mol^{-1})	$\Delta E_{opt}(S)$ (kcal mol^{-1})	$\Delta E_{opt}(R)$ (kcal mol^{-1})	$\lvert\Delta E_{opt}(S) - \Delta E_{opt}(R)\rvert$ (kcal mol^{-1})	$\Delta\Delta E(S)$ (kcal mol^{-1})	$\Delta\Delta E(R)$ (kcal mol^{-1})	$\lvert\Delta\Delta E(S) - \Delta\Delta E(R)\rvert$ (kcal mol^{-1})
χ_4	χ_5	χ_6	χ_{10}									
g^+	g^+	g^+	g^+	257.65	258.41	0.76	250.56	252.14	1.58	7.09	6.27	0.82
g^+	a	g^+	g^+	271.67	264.25	7.42	256.60	255.47	1.13	15.07	8.78	6.29
g^+	a	a	g^+	272.05	264.05	8.00	256.92	255.36	1.56	15.13	8.69	6.44
g^+	a	g^-	g^+	271.76	263.62	8.14	257.24	254.82	2.42	14.52	8.80	5.72
g^+	g^-	a	g^+	266.43	273.26	6.83	257.05	253.46	3.59	9.38	19.80	10.42
g^+	g^-	g^-	g^+	266.15	272.57	6.42	256.76	253.29	3.47	9.39	19.28	9.89
a	g^+	g^+	g^+	271.77	265.24	6.53	255.78	257.02	1.24	15.99	8.22	7.77
a	g^+	a	g^+	272.11	265.31	6.80	256.06	257.13	1.07	16.05	8.18	7.87
a	g^+	g^-	g^+	272.92	265.37	7.55	254.60	256.64	2.04	18.32	8.73	9.59
a	a	g^+	g^+	264.10	271.66	7.56	255.87	261.92	6.05	8.23	9.74	1.51
a	a	a	g^+	264.61	272.01	7.40	256.42	262.21	5.79	8.19	9.8	1.61
a	a	g^-	g^+	264.79	271.66	6.87	256.52	257.96	1.44	8.27	13.7	5.43
a	g^-	g^-	g^+	258.87	258.59	0.28	252.86	252.01	0.85	6.01	6.58	0.57
g^-	a	g^+	g^+	251.81	253.10	1.29	245.51	246.69	1.18	6.30	6.41	0.11
g^-	a	a	g^+	252.34	253.07	0.73	246.17	247.28	1.11	6.17	5.79	0.38
g^-	a	g^-	g^+	252.41	252.42	0.01	246.13	246.48	0.35	6.28	5.94	0.34
g^-	g^-	a	g^+	252.41	251.95	0.46	246.45	245.20	1.25	5.96	6.75	0.79
g^-	g^-	g^-	g^+	252.42	251.57	0.85	246.42	244.58	1.84	6.00	6.99	0.99

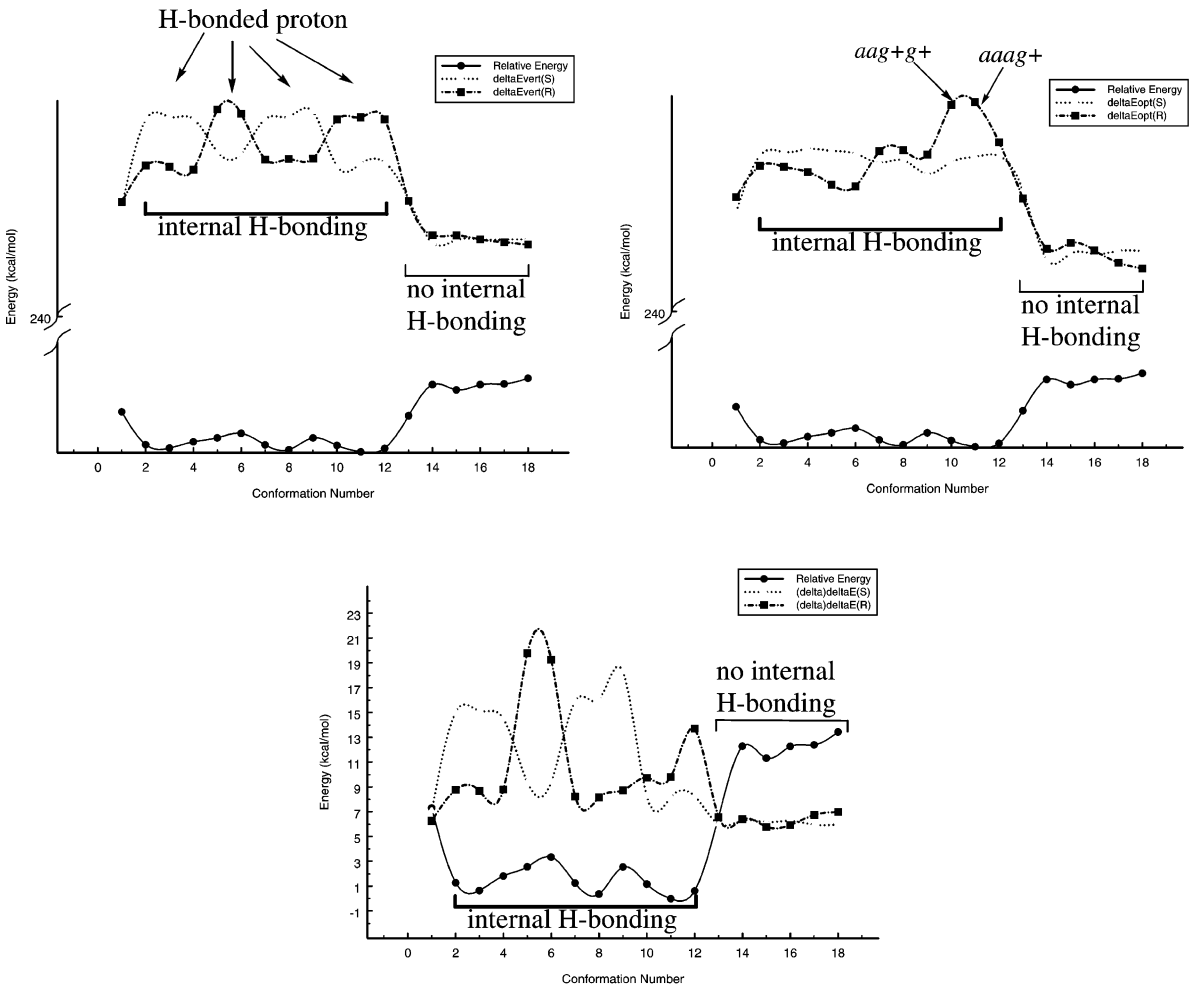

Fig. 7. Trends in $\Delta E_{vert}(S)$ and $\Delta E_{vert}(R)$ (top), $\Delta E_{opt}(S)$ and $\Delta E_{opt}(R)$ (middle), $\Delta\Delta E(S)$ and $\Delta\Delta E(R)$ (bottom) as compared to the relative energy of converged Fragment B conformational minima. (Conformation numbers are defined in Table 3.)

these conformers, the favoured formation of a five-membered ring due to hydrogen bonding between O11 and H_R made the deprotonation of H_R a more energetically demanding task. Deprotonation of these protons from Fragment B would require more energy to overcome the stabilization gained by the five-membered ring.

When analyzing the differences between non-optimized and optimized energies of deprotonation for the conformers, values denoted as $\Delta\Delta E(S)$ and $\Delta\Delta E(R)$ were used to compare the stabilization gained by a respective deprotonated conformer upon optimization (c.f. Table 6). H_S deprotonated conformers: $g^+ag^+g^+$, g^+aag^+, $ag^+g^+g^+$, ag^+ag^+, and $ag^+g^-g^+$; as well as H_R deprotonated conformers: $g^+g^-ag^+$ and $g^+g^-g^-g^+$ all had $\Delta\Delta E$ values greater than 15 kcal mol^{-1} (c.f. Table 6). These high $\Delta\Delta E$ values indicate that the optimized molecular conformation adopted conferred stability to the deprotonated fragment. This trend is similar to the vertical energies of deprotonation. Thus, if the proton abstracted is involved in intramolecular stabilization, then the $\Delta\Delta E$ values would be larger because a more significant molecular geometry rearrangement is necessary. This is opposed to the deprotonation of protons not involved in intramolecular interactions which would

not require major alterations in geometry (c.f. Fig. 7, bottom).

The overall trend shows that conformers devoid of large stabilization interaction had lower energies of deprotonation. This is to say, as the relative conformer energy increased, the SPE and optimized energies of deprotonation decreased (c.f. Fig. 7). Further, conformers with hydrogen bonding had an antagonistic behaviour present for the nitrogen protons; if the H_S proton was involved in hydrogen bonding, then the H_R proton was easily deprotonated and vice versa. Graphically, the latter is displayed as mirror-like increases and decreases in energies of deprotonation for different protons in hydrogen bonded conformers (c.f. conformations 2–12 in Fig. 7, top). However, no such behaviour was evident when no internal hydrogen bonding was present, causing both protons to have comparable energies of deprotonation (c.f. conformations 1, 13–18 in Fig. 7, top).

Calculated (optimized) energies of deprotonation for Fragment B range from the lowest of 244.58 kcal mol^{-1} for the H_R deprotonation of $g^-g^-g^-g^+$ to the highest of 262.21 kcal mol^{-1} for the H_R deprotonation of $aaag^+$. Previous work done on carvedilol has revealed energies of deprotonation of 234 and 238 kcal mol^{-1} for only two conformations of carvedilol, irrespective of the protons deprotonated, at the RHF/6-31G(d) level of theory [11]. These values, given the different basis sets and the fact that two are for whole carvedilol and the rest are for Fragment B, are comparable.

In considering the data, the route with the lowest energy of deprotonation is via the H_R deprotonation of conformer $g^-g^-g^-g^+$ (c.f. Fig. 8). This conformer possessed the highest relative energy of the protonated Fragment B PEHS (13.44 kcal mol^{-1}), lacking internal hydrogen bonding and minimizing the stabilization effect of the ion–dipole interaction

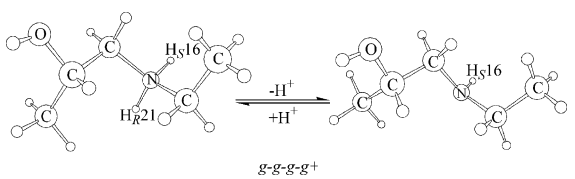

Fig. 8. Route of lowest energy of deprotonation (optimized) is via the H_R deprotonation of conformer $g^-g^-g^-g^+$ (244.58 kcal mol^{-1}).

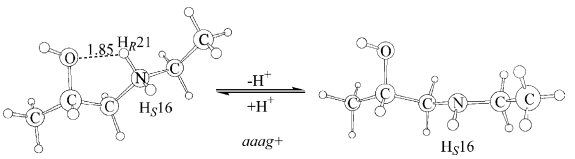

Fig. 9. Route of largest energy of deprotonation (optimized) is via the H_R deprotonation of conformer $aaag^+$ (262.21 kcal mol^{-1}).

between O11 and N5 by having the nitrogen atom and its protons pointing away from the hydroxyl group. As such, deprotonation of either protons was relatively easy

$$|\Delta E_{opt}(S) - \Delta E_{opt}(R)| = 246.42 - 244.58 = 1.84$$

kcal mol^{-1}) because the molecular conformation did not significantly bias any proton. Further, the $\Delta\Delta E$ values indicate that the stabilization gained by the molecular conformation adopted was not substantially large, about 6–7 kcal mol^{-1}.

Contrasting, the $aaag^+$ molecular conformation possessed the largest energy of deprotonation for the deprotonation of its H_R proton ($\Delta E_{opt}(R)$ value of 262.21 kcal mol^{-1}). This conformer also possessed a large difference in energy of deprotonation between the two protons with the H_R proton requiring an additional 5.79 kcal mol^{-1} for deprotonation. The $aaag^+$ conformation was the global minima of the protonated PEHS, possessing a 1.85 Å O11-H_R hydrogen bond forming a five-membered ring (c.f. Fig. 5). As illustrated in Fig. 9, this molecular conformation possesses an inherently difficult H_R deprotonation. Substantial stability was conferred by optimization of the deprotonated conformer as seen with the $\Delta\Delta E$ values (c.f. Table 6).

4. Conclusions

The data therefore indicates that for Fragment B, and extrapolating to carvedilol, events of deprotonation will favour conformations with minimal intramolecular stabilization, and therefore, larger relative energies. This includes minimizing hydrogen bonding and ion-dipole interactions between the positive nitrogen centre and electron lone pairs. Further, it may be expected that abstracted protons will be the ones oriented maximally away from the backbone of

carvedilol and Fragment B as seen with the H_R deprotonation of $g^-g^-g^-g^+$.

This may at first seem somewhat counter-intuitive because the usual emphasis is on finding very stable minima (with low relative energies) as the dominant representatives of PEHS. However, it is imperative that structures with large relative energies are not neglected because the data presented here suggests that different mechanisms will favour different structures. In the carvedilol protonophoretic pathway implicated in the uncoupling of oxidative phosphorylation, molecular conformations with high relative energies will be the best candidates for deprotonation. The latter would be expected especially when once considers that the uncoupling mechanism of proton shuttling requires carvedilol not only to be protonated, but also to be deprotonated upon crossing back into the matrix of the mitochondria. A very stable structure that takes up a proton in the intermembrane space would not be favoured for deprotonation in the matrix. Rather, a structure with minimal stabilization and a decreased basic character would be most accessible to enzymes, substrates, and favoured in protonophoretic pathways as that postulated for carvedilol in the uncoupling of oxidative phosphorylation in the mitochondria.

References

[1] W. Carlson, K.J. Oberg, Cardiovasc. Pharmacol. Ther. 4 (1999) 205.

[2] M. Packer, M.R. Bristow, J.N. Cohn, W.S. Colucci, M.B. Fowler, E.M. Gilbert, N.H Shusterman, N. Engl. J. Med. 334 (1996) 1349.

[3] M.A. Berg, G.A. Chasse, E. Deretey, A.K. Fuzery, B.M. Fung, D.Y.K. Fung, H. Henry-Riyad, A.C. Lin, M.L. Mak, A. Mantas, M. Patel, I.V. Repyakh, M. Staikova, S.J. Salpietro, Ting-Hua Tang, J.C. Vank, A. Perczel, G.I. Csonka, O. Farkas, L.L. Torday, Z. Szekely, I.G. Csizmadia, J. Mol. Struct. (THEOCHEM) 500 (2000) 5.

[4] S. Capomolla, O. Febo, M. Gnemmi, G. Riccardi, C. Opasich, A. Carporotondi, A. Mortara, G. Pinna, F. Cobelli, Am. Heart J. 139 (2000) 596.

[5] M. Metra, S. Nodari, A. D'Aloia, L. Bontempi, E. Boldi, L. Dei Cas, Am. Heart J. 139 (2000) 511.

[6] G. Feuerstein, R.R. Ruffolo Jr., Adv. Pharmacol. 42 (1998) 611.

[7] O. Saijonmaa, K. Metsarinne, F. Fyhrquist, Blood Press. 6 (1997) 24.

[8] G. Feuerstein, T.L. Yue, X. Ma, R.R. Ruffolo, Prog. Cardiovasc. Dis. 41 (1 Suppl 1) (1998) 17.

[9] A.J.F. Searlee, C. Gree, R.L. Wilson, Ellipticines and carbazoles as antioxidants, in: W. Borns, M. Saran, D. Tait (Eds.), Oxygen Radicals and Biology, Walter de Gruyter & Co, Berlin, 1984, pp. 377–381.

[10] D.R. Howlett, A.R. George, D.E. Owen, R.V. Ward, R.E. Markwell, Biochemical Journal 343 (1999) 419.

[11] P.J. Oliveira, M.P. Marques, L.A.E. Batista de Carvalho, A.J.M. Moreno, Biochemical and Biophysical Research Communications 276 (2000) 82.

[12] R.J. Ferrari, Cardiovasc. Pharmacol. 28 (1996) S1.

[13] P.G. Heytler, Uncouplers of Oxidative Phosphorylation, Methods in Enzymology, LV, Academic Press, New York, 1979, pp. 462-472.

[14] A. Tzagoloff, Mitochondria, Plenum Press, New York, 1982.

[15] S.S. Korshunov, V.P. Skulachev, A.A. Starkov, FEBS Lett. 416 (1997) 15.

[16] H.G. Oldham, S.E. Clarke, Drug Metab. Dispos. 25 (1997) 970.

[17] R.R. Ruffolo Jr., M. Gellai, J.P. Hieble, R.N. Willette, A.J. Nichols, Eur. J. Clin. Pharmacol. 38 (1990) S82.

[18] R. Feuerstein, T.L. Yue, Pharmacology 48 (1994) 385.

[19] T.L. Yue, P.J. Mckenna, P.G. Lysko, J.L. Gu, K.A. Lysko, R.R. Ruffolo Jr., G.Z. Feuerstein, Eur. J. Pharmacol. 251 (1994) 237.

[20] D.R.P. Almeida, L.F. Pisterzi, G.A. Chass, L.L. Torday, A. Varro, J. Gy. Papp, I.G.J. Csizmadia, Phys. Chem. A 106 (43) (2002) 10423.

[21] M.J. Frisch, G.W. Trucks, H.B. Schlegel, G.E. Scuseria, M.A. Robb, J.R. Cheeseman, V.G. Zakrzewski, J.A. Montgomery, Jr., R.E. Stratmann, J.C. Burant, S. Dapprich, J.M. Millam, A.D. Daniels, K.N. Kudin, M.C. Strain, O. Farkas, J. Tomasi, V. Barone, M. Cossi, R. Cammi, B. Mennucci, C.Pomelli, C. Adamo, S. Clifford, J. Ochterski, G.A. Petersson, P.Y. Ayala, Q. Cui, K. Morokuma, D.K. Malick, A.D. Rabuck, K. Raghavachari, J.B. Foresman, J. Cioslowski, J.V. Ortiz, A.G. Baboul, B.B. Stefanov, G. Liu, A. Liashenko, P. Piskorz, I. Komaromi, R. Gomperts, R.L. Martin, D.J. Fox, T. Keith, M.A. Al-Laham, C.Y. Peng, A. Nanayakkara, C. Gonzalez, M. Challacombe, P.M.W. Gill, B.G. Johnson, W. Chen, M.W. Wong, J.L. Andres, M. Head-Gordon, E.S. Replogle, J.A. Pople, GAUSSIAN 98 (Revision A.9), Gaussian, Inc., Pittsburgh PA, 1998.